

Numerical Investigation of Flow Structure around NACA 0018 with Slot

Omer Fethi ASAN¹, Emre GULER², Muhammed Murat AKSOY³, Engin PINAR⁴, Tahir DURHASAN^{5*}

¹Adana Alparslan Türkeş Science and Technology University, Aeronautics and Astronautics Faculty, Aerospace Engineering, 01250, Adana

²Tarsus University, Aeronautics and Astronautics Faculty, Aerospace Engineering, 33400, Mersin

³Osmaniye Korkut Ata University, Engineering Faculty, Energy Systems Engineering, 80000, Osmaniye

⁴Cukurova University, Ceyhan Engineering Faculty, Mechanical Engineering, 01950, Adana

⁵Adana Alparslan Türkeş Science and Technology University, Aeronautics and Astronautics Faculty, Aerospace Engineering, 01250, Adana

¹<https://orcid.org/0000-0001-7982-2282>

²<https://orcid.org/0000-0001-7337-8678>

³<https://orcid.org/0000-0001-7594-9462>

⁴<https://orcid.org/0000-0002-7484-8616>

⁵<https://orcid.org/0000-0001-5212-9170>

*Corresponding author: tdurhasan@atu.edu.tr

Research Article

Article History:

Received: 18.11.2022

Accepted: 12.06.2023

Published online: 20.12.2023

Keywords:

Airfoil

CFD

Reynolds number

Slot

Passive flow control

ABSTRACT

A numerical investigation was performed on NACA 0018 airfoil with slot at various angles of attack. The computational fluid dynamics (CFD) results were compared with the base airfoil to show the effectiveness of the airfoil. Reynolds number was kept constant as $Re=3 \times 10^5$ to thoroughly understand how different locations of slot would provide passive flow control from aerodynamic perspective. Three different slot locations were used to reveal the effectiveness of the slot compared to the base airfoil for higher angles of attack. The results show that the slotted design would yield to increase the lift and to delay the stall angle of base airfoil.

Yarık açılan NACA 0018 Etrafındaki Akış Yapısının Sayısal İncelenmesi

Araştırma Makalesi

Makale Tarihi:

Geliş tarihi: 18.11.2022

Kabul tarihi: 12.06.2023

Online Yayınlanma: 20.12.2023

Anahtar Kelimeler:

Kanat profili

HAD

Reynolds sayısı

Yarık

Pasif akış kontrolü

ÖZ

Çeşitli hücum açılarında slotlu NACA 0018 kanat profili üzerinde sayısal bir inceleme yapılmıştır. Hesaplamalı akışkanlar dinamiği (CFD) sonuçları, kanat profilinin etkinliğini göstermek için temel kanat profili ile karşılaştırıldı. Farklı yarık konumlarının aerodinamik perspektiften pasif akış kontrolünü nasıl sağlayacağını iyice anlamak için Reynolds sayısı $Re = 3 \times 10^5$ olarak sabit tutuldu. Daha yüksek hücum açıları için temel kanat profiline kıyasla yarıkların etkinliğini ortaya çıkarmak için üç farklı yuva konumu kullanılmıştır. Sonuçlar, yarıklı tasarımın kaldırma ve temel kanat profilinin perdövites açısını geciktirmeye yol açacağını göstermektedir.

To Cite: Asan OF., Güler E., Aksoy MM., Pinar E., Durhasan T. Numerical Investigation of Flow Structure around NACA 0018 with Slot. Osmaniye Korkut Ata Üniversitesi Fen Bilimleri Enstitüsü Dergisi 2023; 6(Ek Sayı): 152-167.

Introduction

The fundamental purpose of an airfoil is to create a lift to the attached body with the help of pressure difference between the upper and lower surfaces of it. The pressure distribution over an airfoil is one of the important optimization topics in the flight industry. To enhance the ability of lifting, the flow

structure at the upper surface of airfoils (suction surface) has been studied to control and to minimize the turbulence effects that yields to stall the flight operation and worse conclusions.

Since there are many airfoil shapes (Güzelbey et al., 2018) for different flow types, the flow structure around of the airfoils has been analyzed and also modified using active or passive flow control techniques to enhance the aerodynamic performance. The main goal of the flow control is to achieve a higher angle of attack (α) (i.e., the angle between flow direction and chord line) without stall condition. For active flow control techniques, we need an external energy input to the boundary of the airfoil such as using synthetic jets, actuators, control sensor tools, suction, and blowing (Abbasi and Souri, 2020; Aley et al., 2020; Ohashi et al., 2020; Maldonado et al., 2021).

For passive control, various modifications applied to the airfoil geometry are available in the literature. The manipulation with the geometrical structure of airfoils provides us to prevent the vortex shedding at near wake of the trailing edge that leads to increase the lift and the angle of attack. Gurney flap is one of the common methods to reduce the separation vortices at the upper side of the airfoil to increase the lift forces (Wang et al., 2008). By attaching Gurney flap to NACA 4412, the maximum lift coefficient (C_L) has been raised from 1.49 up to 1.96. Also, when the height of Gurney flap (h) is arranged to 1.25% of chord length (i.e., $h=1.25\%c$), the maximum C_L is enhanced 36% at the angle of attack of 17° . Hence, with the help of high lift forces, drag coefficient (C_D) is decreased (Storms and Jang, 1994). By comparing NACA 0011 and NACA 4412 with Gurney flap, there has been an raise in the ratio of lift to drag coefficient (C_L/C_D) for the NACA 0011 which enhances the aerodynamic performance unlike the NACA 4412 (Singh et al., 2007). The splitter plate is also used to advance the flight conditions of airfoils. The observed improvements are likely for airfoils such as NACA 0012 (Ozkan, 2021), FB-3500-1750 (Metzinger et al., 2018), and even for wind turbine airfoils such as DU97-W-300 (Song, 2020). For instance, based on three different splitter plates' locations at the trailing edge, it is revealed that the adverse influences of the vortex shedding near wake of the NACA 0012 airfoil has been significantly reduced for full stall condition (i.e., $\alpha=16^\circ$) at Reynolds number, $Re=20,000$ (Ozkan, 2021).

Moreover, slotted airfoils are utilized to improve aerodynamic performance for base NACA airfoil models. The location of slot is mostly chosen on the front side of the airfoil. To control the laminar separation bubble (LSB), two types of slots are investigated for NACA 0021 and a 4% rise on the C_L is observed as well as decreasing the length of LSB (Ramzi, 2018). Beyhaghi and Amono have conducted both experimental and numerical studies on slotted NACA 4412, and their results provide us that C_L could be raised up to 30% without a drag penalty (Beyhaghi and Amano, 2018). For an optimum propeller design, Mohamed et al. have numerically studied different slotted NACA airfoils and compared its results with the base airfoils. Their findings show that a slotted design is not always working properly from the performance perspective. Additionally, their comprehensive results lead that if the aerodynamic characteristic of the airfoil is constructed for high Re number and high lift, the slotted propeller would work efficiently (Mohamed et al., 2021). Therefore, for the flight efficiency

(i.e., high Re numbers and high lift characteristic are needed), slotted design of an airfoil usually gives us beneficial results. For NACA 0018 airfoil, the slotted design would be effective to control the flow at near wake of the body by preventing boundary layer separation (Mohamed et al., 2020).

Even though aforementioned airfoil studies with slot reveal good efficiency for the flight conditions, the enhancement on the slot design variations would still yield to control the unfavorable effects of turbulent flows. Thus, the flow structure of NACA 0018 airfoil with slot was numerically investigated in this paper. The effects of these three slotted models are discussed further and compared with the base airfoil to reveal how an airfoil with a slot would bring in a high lift coefficient as well as delay the stall angle.

Material and Method

Model and Computational Grid

The computational fluid dynamics (CFD) analysis was numerically accomplished using ANSYS Fluent for NACA 0018 airfoil. For CFD problems, ANSYS Fluent is commonly used to investigate the flow structures (Hussein et al., 2021; Öztürk and Demircan, 2022). In this 2-D problem, k- ω SST turbulence model was used (Menter, 1994) to solve the flow structure effectively. In this computational experiment, the Reynolds number was kept constant to $Re=3 \times 10^5$. Reynolds number is defined as $\rho V_\infty L / \mu$, where ρ , V_∞ , and μ are density of the fluid, freestream velocity of the fluid, and dynamic viscosity of the fluid, respectively. L is the characteristic length in which it is the chord length (c) of the airfoil. The chord length, c , was taken as 150 mm. Several dimensionless parameters have been reproduced in order to have an idea about the performance of the wings such as drag coefficient (C_D), pressure coefficient (C_p) lift coefficient (C_L). The pressure distribution around the airfoil can be dimensionless by using Equation 1 and the dimensionless number is called as the pressure coefficient (C_p). In the equation; p is the static pressure of the measuring point on the body, p_∞ is the static pressure of the freestream flow, v_∞ is the velocity of the freestream flow, and ρ is the density of the fluid.

$$C_p = \frac{p - p_\infty}{\frac{1}{2} \rho V_\infty^2} \quad (1)$$

Lift and drag coefficients are calculated by using Equation 2 and Equation 3, respectively. In the equations, F_L and F_D are lift and drag forces, respectively and A is reference area.

$$C_L = \frac{F_L}{\frac{1}{2} \rho V_\infty^2 A} \quad (2)$$

$$C_D = \frac{F_D}{\frac{1}{2} \rho V_\infty^2 A} \quad (3)$$

All solutions were operated at steady-state solution with using coupled-implicit algorithm scheme was operated for density-based solver. For gradient, the least square cell-based method was used. For

spatial discretization, second order upwind method was utilized. No-slip wall boundary condition was applied for airfoil. Also, the flow region was chosen as pressure far-field condition by 5% of turbulent intensity and 0.1992 m of hydraulic diameter. Residuals for parameters were set to 10-8 convergence absolute criteria.

Various fluid domains are created for base NACA 0018 airfoil (i.e., without slot) to compare it with the current literature for the validation study, and three slotted airfoils. Also, the effect of outlet slot location was examined at different angles of attack ($\alpha=0^\circ, 4^\circ, 6^\circ, 8^\circ, 10^\circ, 12^\circ, 13^\circ, 14^\circ, 15^\circ, 16^\circ, 17^\circ, 18^\circ, 19^\circ$ and 20°). The schematic presentation of slotted NACA 0018 airfoil is shown in Figure 1. The parameters in Figure 1 represented the chord length (c), the width of slot outlet ($W1$), the width of slot inlet ($W2$), the angle of attack (α), and the radius of the inlet and outlet slot (R). The distance between the midpoint of the slot's width and leading-edge point was shown as $L1$ and $L2$ for upper and lower surfaces of the airfoil, respectively.

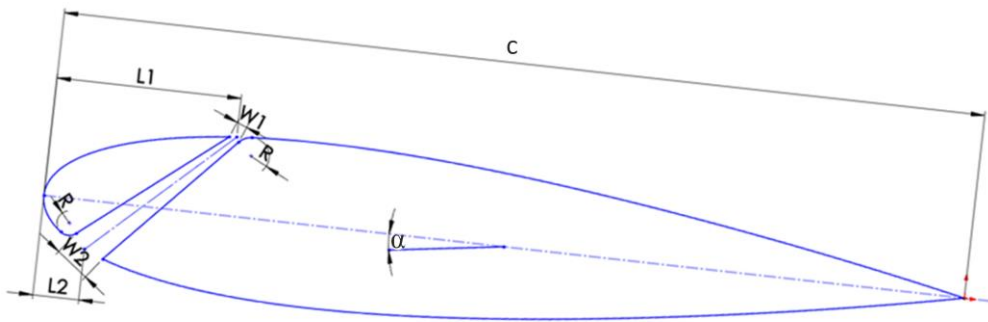


Figure 1. Schematic view of slotted NACA 0018 airfoil.

To create three different slotted airfoils, firstly, the ratio of $W2/W1$ was kept as 4.0 (Belmadi et al., 2016) and the inlet position of the slot ($L2$) was kept constant at 5% of the chord length. Then, $L1$ length was changed for three different locations as defining a new variable, x , with respect to the ratio of chord length (x/c). Thus, the slot outlet was located at 20%, 40%, and 60% of total chord length for three different slots. The details of the test cases for the slotted airfoil were given in Table 1. It was referred to $x/c=20\%$, $x/c=40\%$, and $x/c=60\%$ models as Model 20, Model 40, and Model 60, respectively, hereafter. We would present these slotted models in Figure 2 in detail.

Table 1. Test cases of slotted airfoil

Parameters	Model 20	Model 40	Model 60
$W1/c$	1%	1%	1%
$L1/c$	20%	40%	60%
$L2/c$	5%	5%	5%
$W2/W1$	4	4	4
R/c	2%	7%	18%

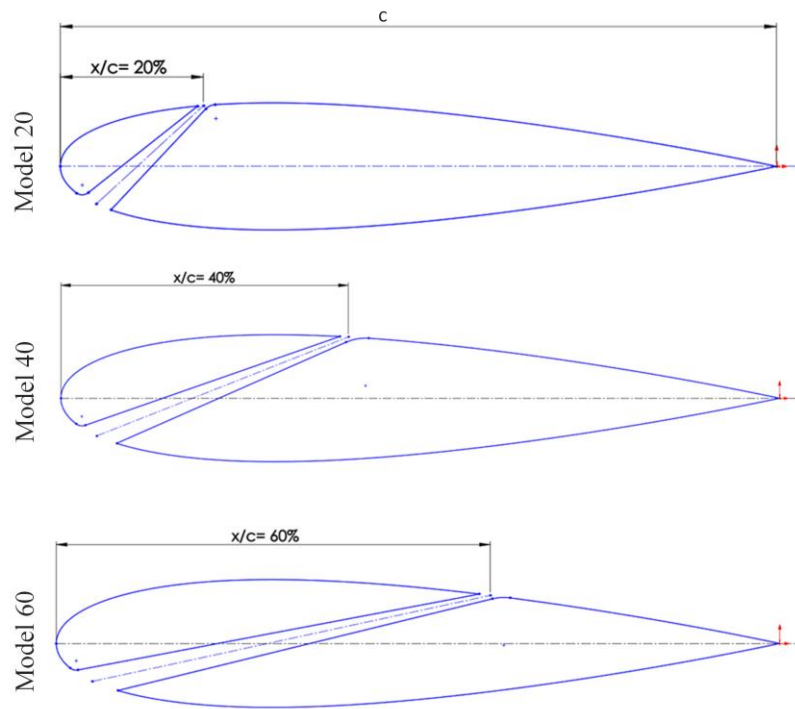


Figure 2. Schematic view of different configurations of slotted NACA 0018 airfoil.

For the computational grid, the C-type mesh structure was used for providing a more uniform distribution around the airfoil and to predict the boundary layer flows efficiently. The fluid domain was designated as $12.5c$ and $25c$ for y -axis and x -axis directions, respectively. Hence, the effect of the wall to the flow structure would be prevented. The grid structure is shown in Figure 3 for slotted airfoil for 200,000 cells. The y^+ value was set to less than 1 and the growth rate was set as 1.2. The mesh element size was formed smaller along the airfoil due to achieve plausible results.

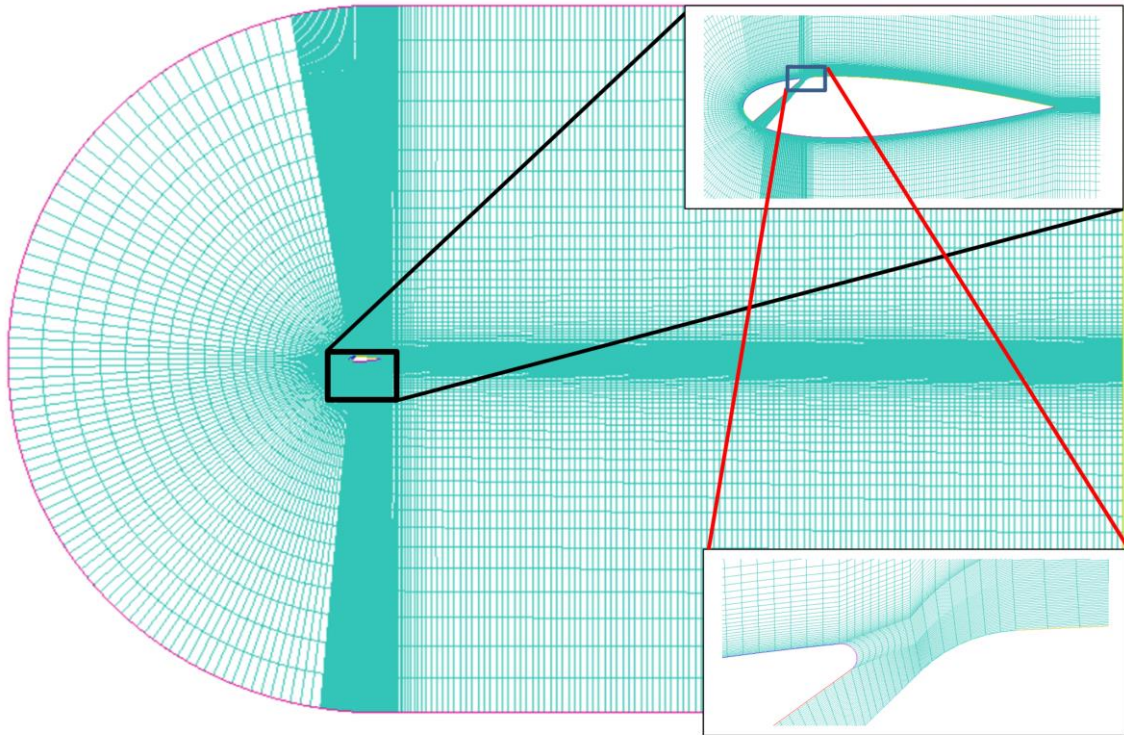


Figure 2. The mesh grid of slotted NACA 0018 airfoil.

Validation

At the angle of attack of $\alpha=10^\circ$, five different element numbers were examined for base airfoil. It was conducted with k- ω SST turbulence model to compare the obtained lift coefficients with both experimental (Jacobs, 1937; Timmer, 2008) and numerical studies (Shabur et al., 2021) as seen in Figure 3.

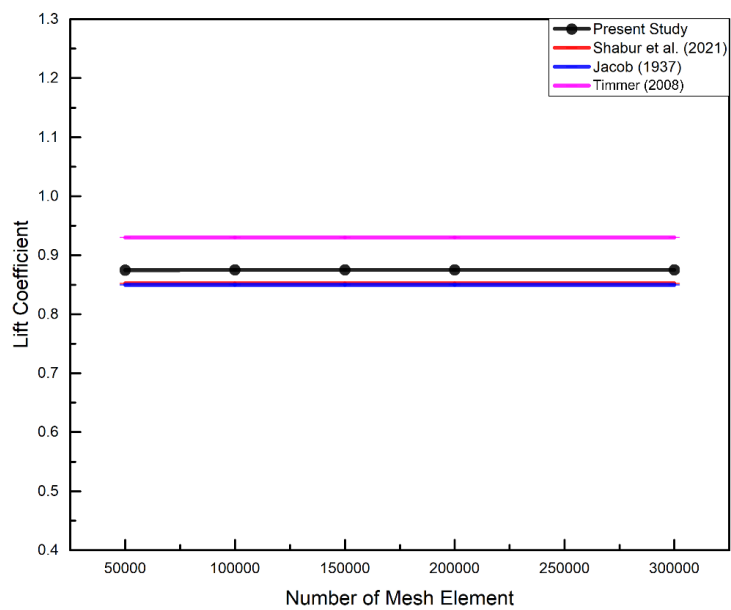


Figure 3. Mesh independence study.

It is clearly seen from Figure 3 that the increase in the number of mesh elements would not affect lift coefficient significantly. In the present study, the number of mesh elements was taken to be 100,000 since the C_L was nearly the same with the experimental results. Figure 4 reveals the value of C_L with respect to α for both present study and studies available in the literature, and it is clearly seen that the curve of the present study has overlapped with experimental data (Jacobs, 1937; Timmer, 2008). The maximum error is approximately 12% obtained for post stall angle ($\alpha=16^\circ$)

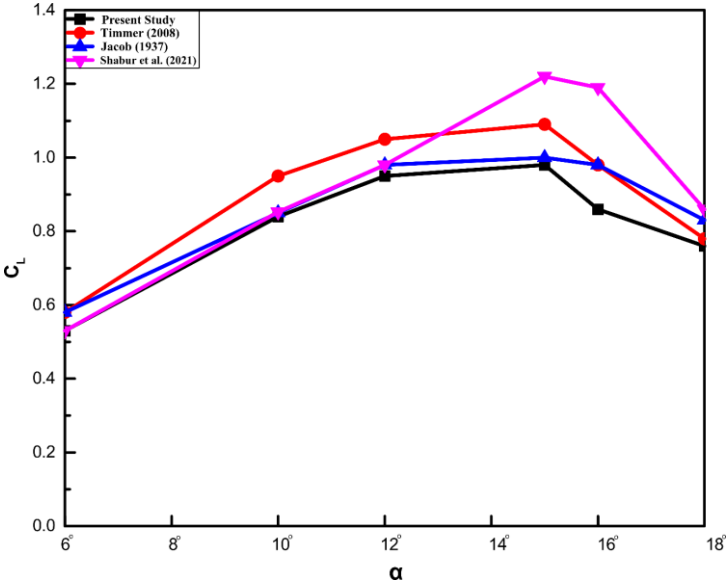


Figure 4. Comparison of experimental results with this study.

Results and Discussion

It is presented the lift and drag coefficients for both slotted models and base NACA 0018 airfoil at various angles of attack. Figure 5 shows the variation of the lift coefficient (C_L) with respect to the angle of attack (α) for different slotted configurations (i.e., Model 20, Model 40, and Model 60) and the base case. Since NACA 0018 airfoil has a symmetrical geometry, the value of lift coefficient enhances with the increasing angle of attack up to a point for all cases. For the base case, the maximum value of C_L is 0.99 at $\alpha=14^\circ$. It is clearly seen from Figure 5 that a sudden decrease in the lift coefficient to $C_L=0.86$ was observed at the angle of attack of $\alpha=16^\circ$ due to the stall condition. For the slotted models, all models could not achieve a higher lift coefficient than the base airfoil up to the angle of attack of $\alpha=6^\circ$, because of having an impaired aerodynamic structure for lower α . However, the value of lift coefficient enhances as the angle of attack raise. The C_L values of Model 60 are slightly higher than Model 20 and Model 40 at lower angles of attack, and Model 60 was delayed the stall angle 3° compared to the stall angle of base airfoil which is $\alpha=16^\circ$. It is observed the accomplishment of Model 40 after $\alpha=15^\circ$ from the lift force perspective, and the stall angle is also delayed around 4° . The maximum C_L is obtained as 1.6 at angle of attack of $\alpha=19^\circ$ for Model 40. It is observed that maximum C_L value of Model 40, and raised by about 150% compared to the maximum C_L of base airfoil. As a result, it is revealed that Model 40 yields good results by delaying the stall

angle as well as providing higher C_L . For Model 20, it is clearly seen that the most delayed stall angle is as opposed to other slotted models. Yet, C_L values are not higher prior to the stall points of Model 40 and Model 60.

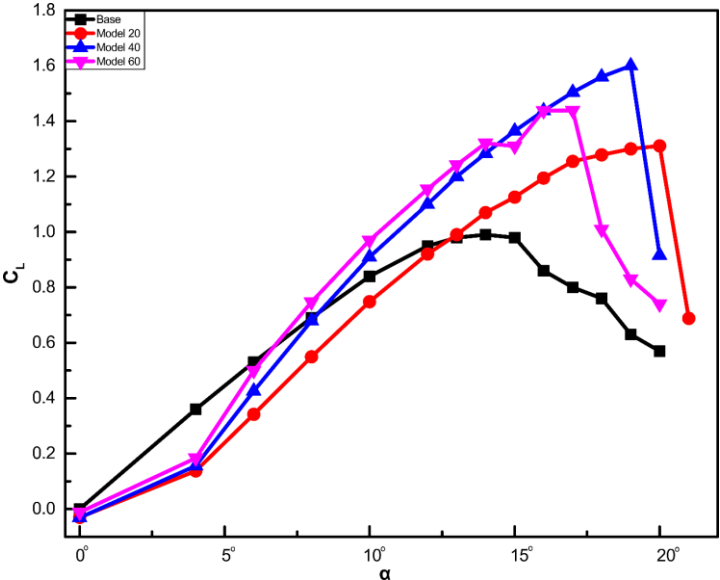


Figure 5. The variation of lift coefficients with angles of attack.

Figure 6 depicts the drag coefficients (C_D) at various angles of attack. For the base airfoil, the drag coefficient is calculated as $C_D=0.017$ at zero angle of attack. Since the front cross-sectional area of the airfoil increases at higher angles of attack, it is interpreted that the relationship between the angle of attack and the drag force is directly proportional. The drag force is sharply enhanced about 200% after the stall, $\alpha=16^\circ$, for base airfoil. As expected for the slotted models, modifying the geometrical structure would cause to raise the drag force. Hence, up to $\alpha=10^\circ$, higher C_D is observed compared to the base case. Even though the stall angle is delayed for the slotted models, it is observed that the higher C_D values prior to the stall angle of the base airfoil. Furthermore, Model 40 would provide the slowest increase of values with respect to other models.

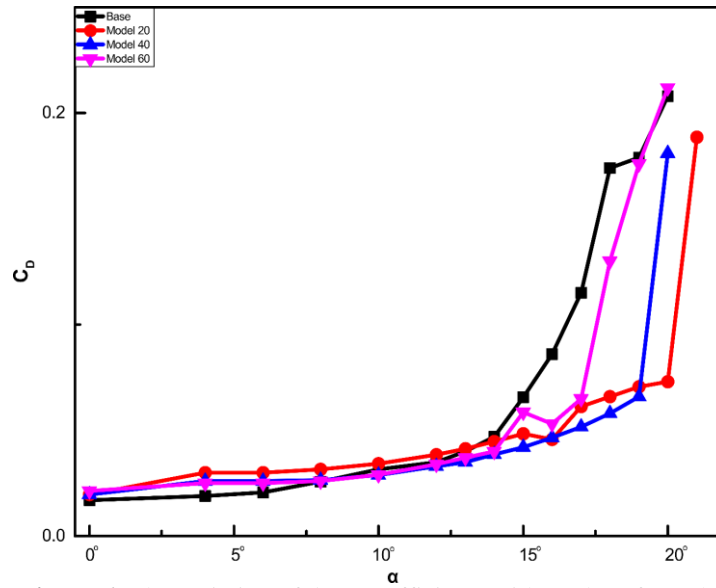


Figure 6. The variation of drag coefficients with angles of attack.

It is showed the pressure coefficient (C_p) values at $12^\circ \leq \alpha \leq 19^\circ$ to present the pressure distribution around the airfoil in Figure 7. It is worth noting that the slotted airfoils have two pressure distribution parts; the front and rear parts of the slotted airfoil are represented as red and blue lines, respectively. The black line shows the data for base airfoil. Firstly, it is observed that the peak magnitude of pressure is decreased for base airfoil when angle of attack increases from 15° to 17° due to the stall condition. This situation is more distinct at $\alpha=19^\circ$. It is clearly seen from Figure 7 that slotted model remarkably delays the stall angle in comparison with the base airfoil, and also enhancing of the lift force is dominated by rear part of airfoil for the slotted models. Also, another inconsistency in terms of the peak of the C_p graph is observed for Model 60 at $\alpha=19^\circ$. Even though the pressure increases for closer locations of the slot's outlet towards the trailing edge, it is seen from Figure 7 that the pressure of the Model 60 decreases in which slot's outlet was located closest to the trailing edge compared to Model 20 and 40. This phenomenon might be explained better by interpreting Figure 9 because it gives rise to the recirculation region at $\alpha=19^\circ$ for Model 60.

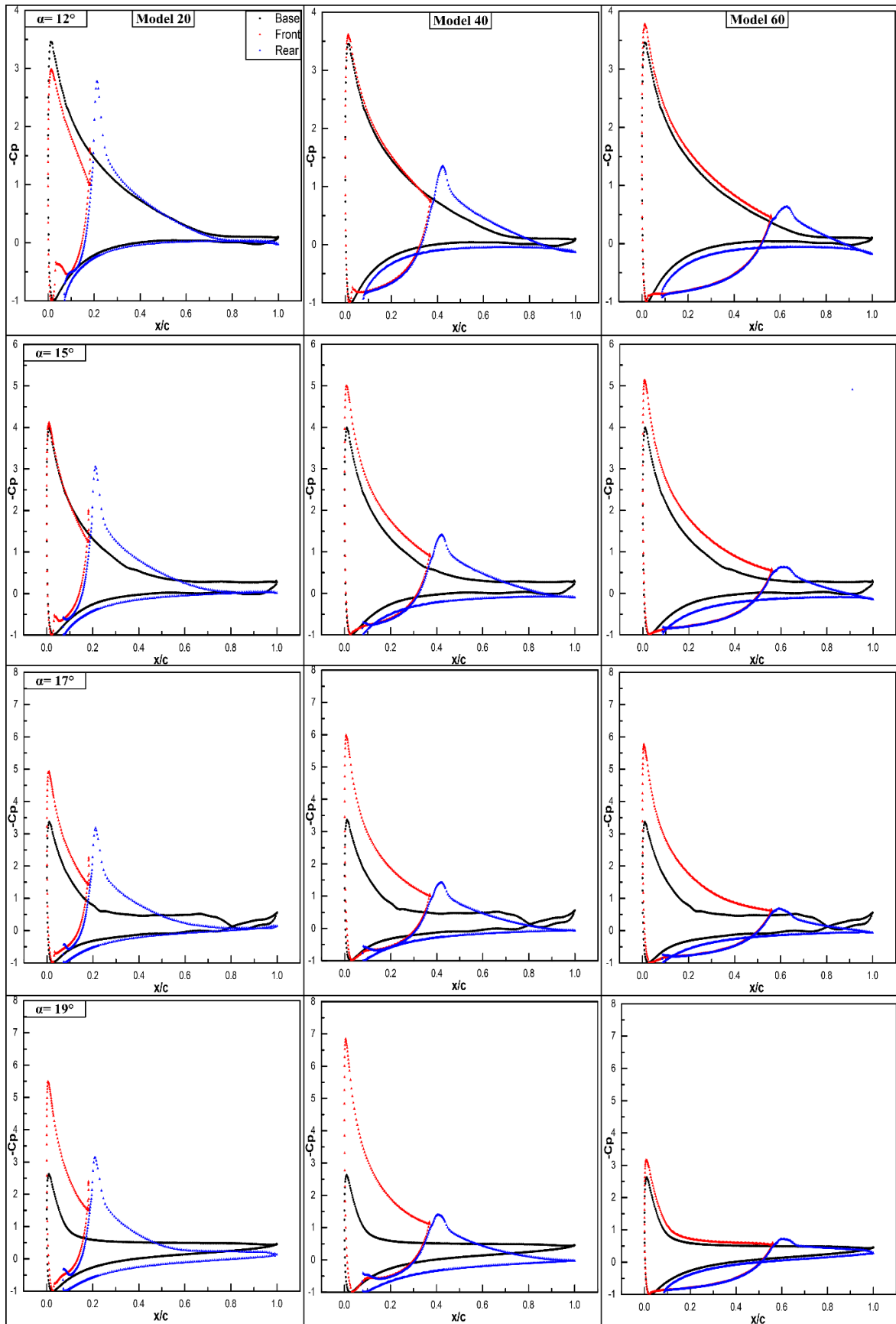


Figure 7. The pressure coefficient distributions at $12^\circ \leq \alpha \leq 19^\circ$.

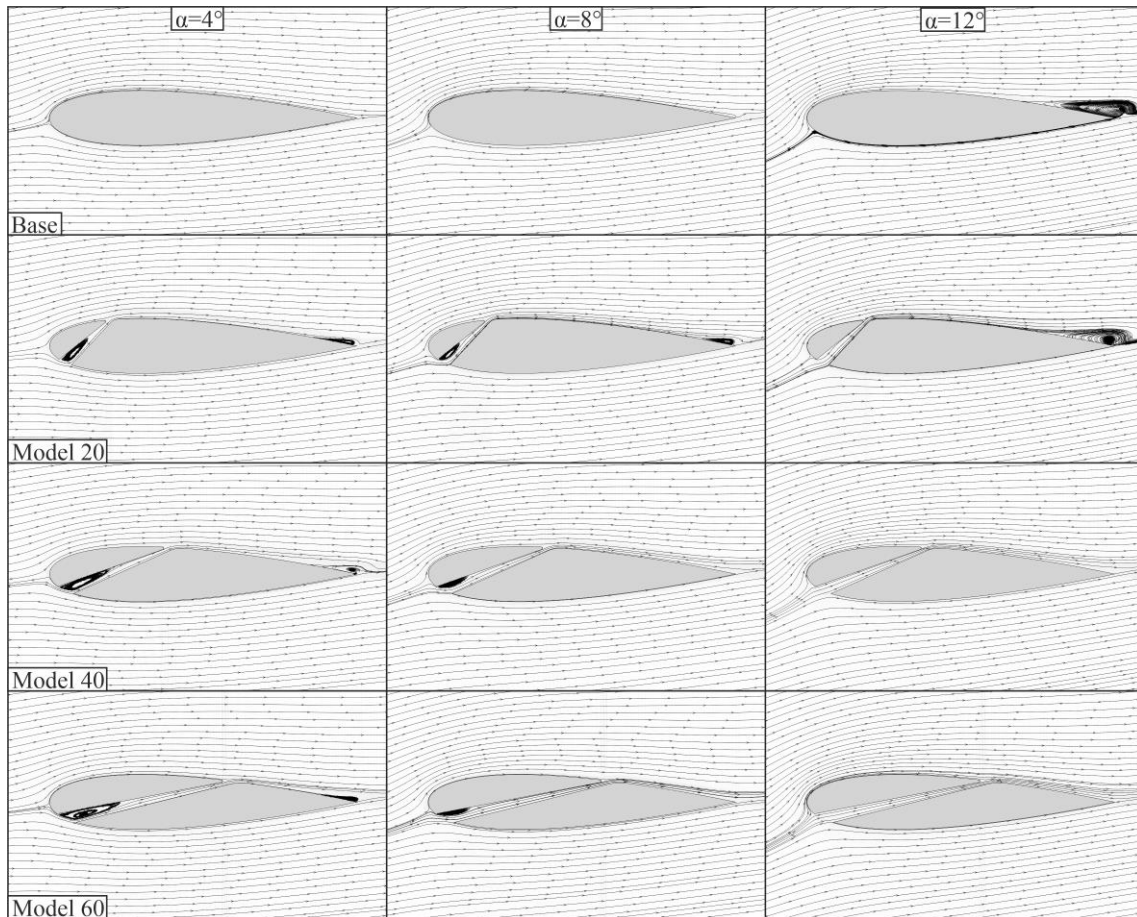


Figure 8 a. The streamlines of airfoils at $4^\circ \leq \alpha \leq 12^\circ$.

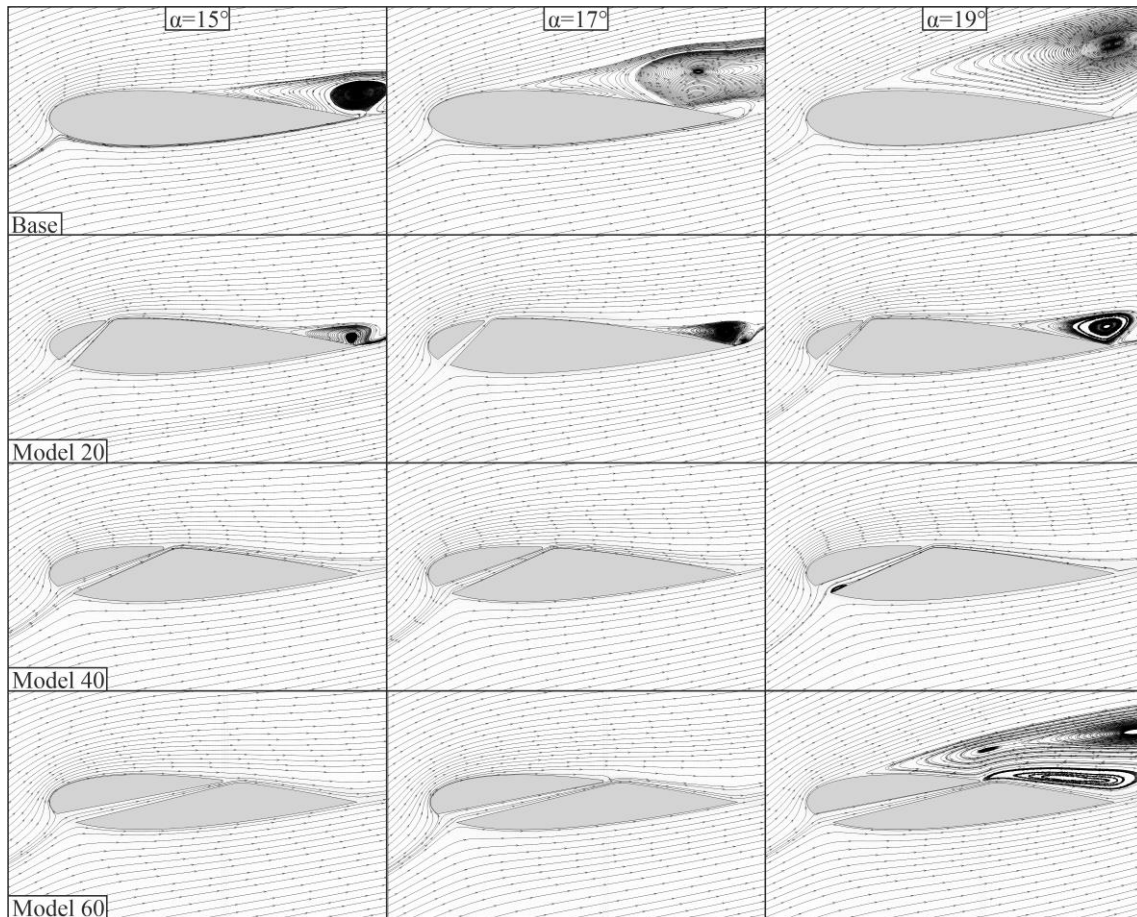


Figure 8 b. The streamlines of airfoils at $15^\circ \leq \alpha \leq 19^\circ$.

Figure 8a and 8b represent the streamline topologies at angles of attack of 4° , 8° , 10° , 12° , 15° , 17° and 19° . At $\alpha=4^\circ$, streamline patterns indicate that flow follows the airfoil surface for all models. For Model 40 and 60, small foci (which indicates the recirculation region) observed in the slot. A slight trailing edge separation appears for base airfoil at $\alpha=12^\circ$, while it is more distinct at $\alpha=15^\circ$. Furthermore, laminar separation bubble is not observed for the base airfoil similar with the literature. For the base airfoil, the separation point is closer to the leading edge with the increase in the angle of attack and the recirculation region covers the suction surface of the airfoil. The trailing edge separation is also observed for Model 20 at $\alpha=15^\circ$. On the contrary, the foci formation on the trailing edge is not observed for Model 40 and 60 because the momentum transfer from slot's outlet to the trailing edge prevents the edge separation. The size of recirculation region increases at $\alpha=17^\circ$ and 19° , but it is still smaller than base airfoil. The trailing edge separation and the recirculation region on the section surface is not observed for Model 40 at all angles of attack as a satisfactory result of the flow control. From this point of view, it can be concluded that model 40 is the most successful model for all angles of attack when compared to the other models.

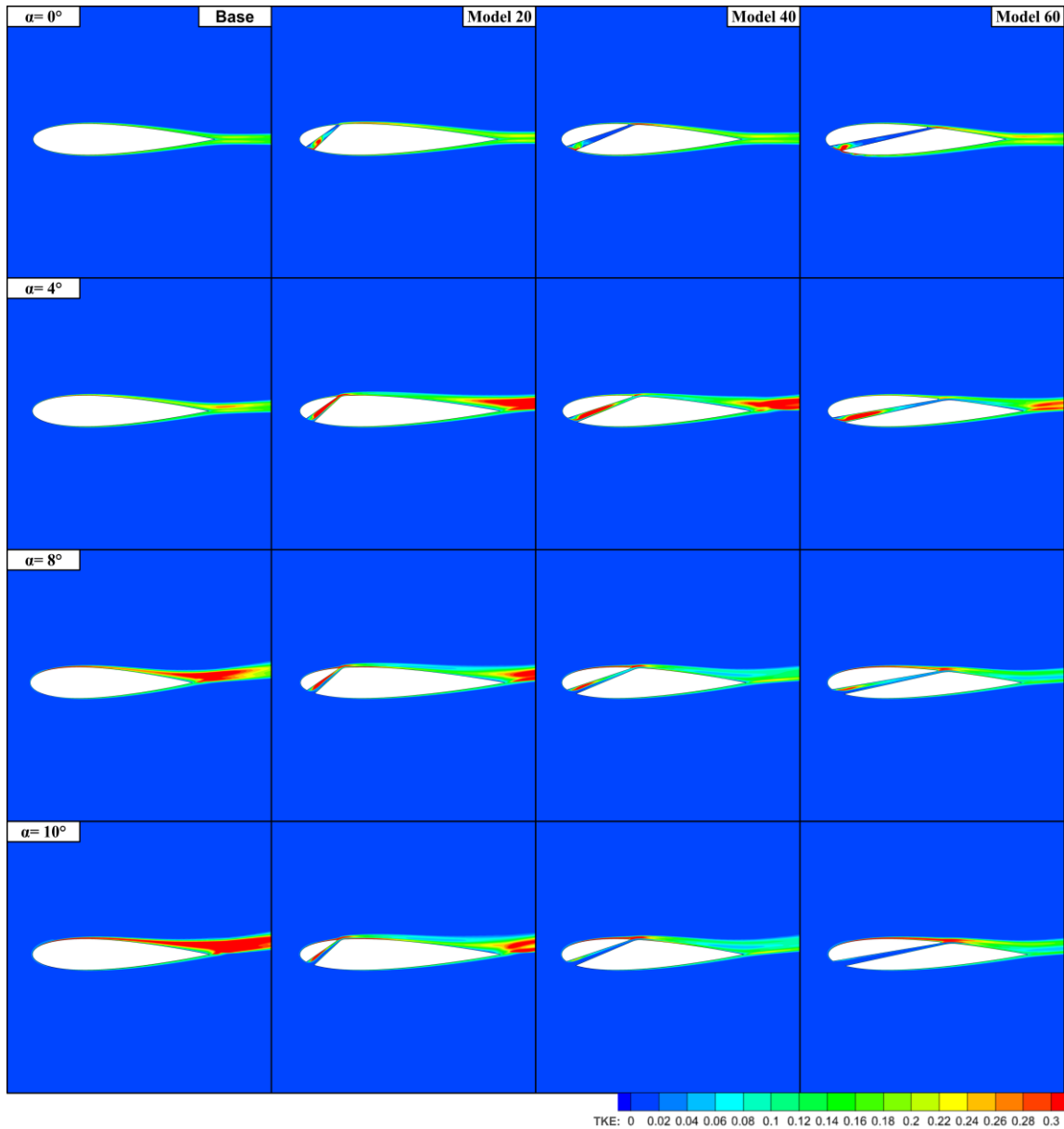


Figure 9a. Turbulence kinetic energy contours for $0^\circ \leq \alpha \leq 10^\circ$.

Figure 9a and 9b show the turbulent kinetic energy (TKE) contours for all airfoils at different angles of attack. For Figure 9a, the peak magnitude of TKE occurs at inlet and outlet of the slot due to the flow separation inside the slot region. At $\alpha=4^\circ$, the existence of the slot adversely affects the flow patterns and the peak magnitude of TKE remarkably increases in near wake region in comparison with base airfoil. The effect of slot on the suppression of TKE is observed at $\alpha=8^\circ$ especially for Model 40 and 60. For high angles of attacks, the effect of slot on the suppression of TKE is more apparent when compared to the base airfoil. It is clearly seen that TKE is remarkably suppressed at $\alpha \geq 10^\circ$. Especially after the angle of attack of $\alpha = 15^\circ$, the very intense red region behind the base airfoil in the contour indicates the severeness of produced TKE. While the turbulence intensities of Model 20 and Model 60 are similar to each other, turbulence intensity occurred in Model 40 is minimal. It can be concluded that flow control around the airfoil can be achieved with the help of the slot design for high angles of attack.

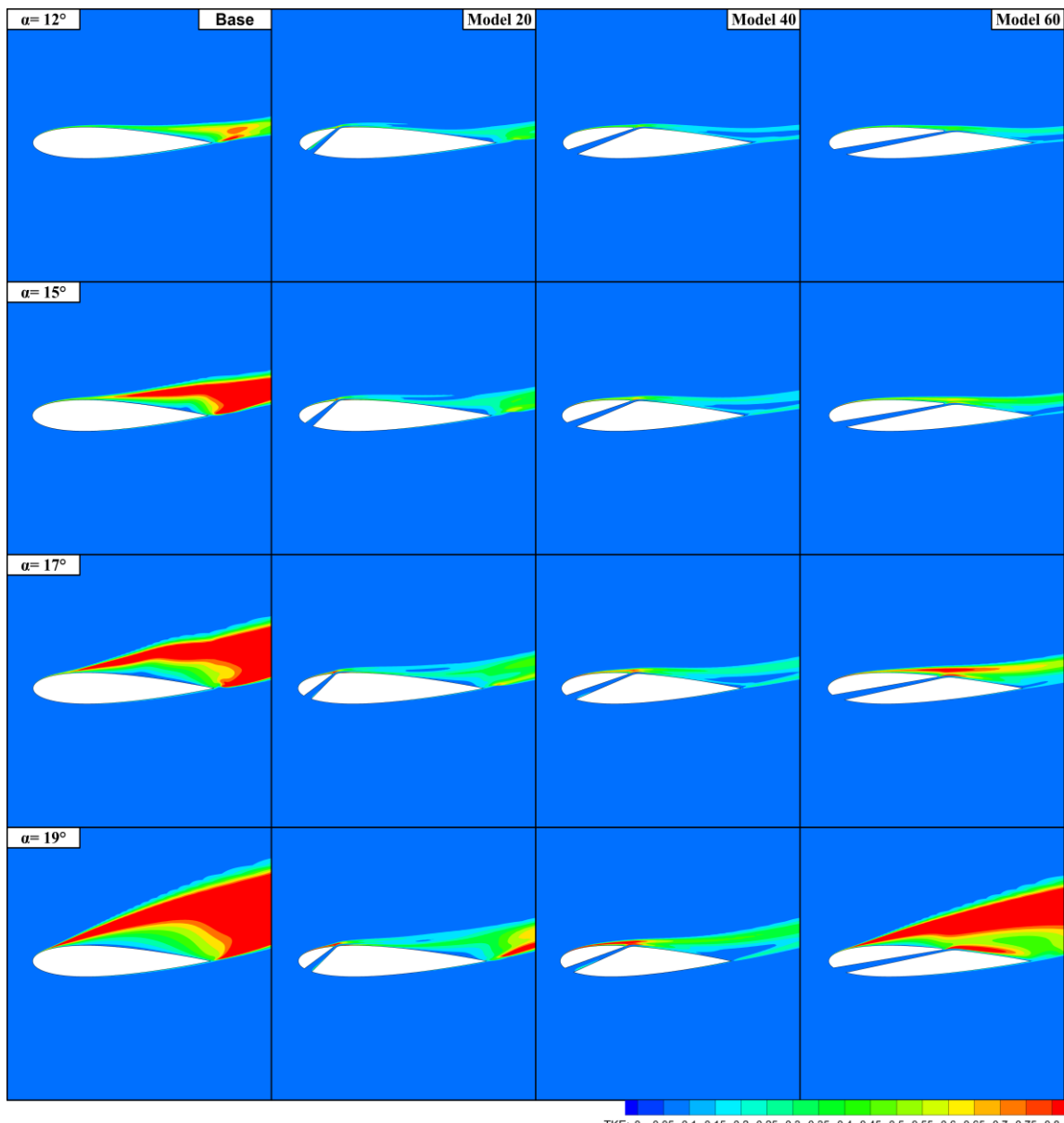


Figure 9b. Turbulence kinetic energy contours for $12^\circ \leq \alpha \leq 19^\circ$.

Conclusion

The aim of study is to control the recirculation area formed behind an airfoil by using slots at high angles of attack, α . Therefore, NACA 0018 airfoil is numerically analyzed and slotted for different chordwise locations at $Re=3 \times 10^5$ and $0^\circ \leq \alpha \leq 20^\circ$. The provided results were compared with base airfoil due to reveal the effect of slot on flow characteristic and aerodynamic performance. The three slotted models are created, namely Model 20, Model 40, Model 60, by changing the outlet location of the slot. In general, it is observed that all slotted models provide us to delay the stall angle of base airfoil as well as higher lift forces for high angles of attack. To comparison with the slotted models, Model 40 gives us the efficient lift results by annihilating the recirculation region of base airfoil at $\alpha=19^\circ$, and it also yields to delay the stall angle by 4° compared to the base airfoil.

Conflict of Interest

Authors have declared no conflict of interest.

Author's Contributions

The authors declare that they have contributed equally to the article.

References

- Abbasi S., Souri M. Reducing aerodynamic noise in a rod-airfoil using suction and blowing control method. *International Journal of Applied Mechanics* 2020; 12: 2050036.
- Aley KS., Guha TK., Kumar R. Active flow control of a high-lift supercritical airfoil with microjet actuators. *AIAA Journal* 2020; 58: 2053–2069.
- Belamadi R., Djemili A., Ilinca A., Mdouki R. Aerodynamic performance analysis of slotted airfoils for application to wind turbine blades. *Journal of Wind Engineering and Industrial Aerodynamics* 2016; 151: 79–99.
- Beyhaghi S., Amano RS. A parametric study on leading-edge slots used on wind turbine airfoils at various angles of attack. *Journal of Wind Engineering and Industrial Aerodynamics* 2018; 175: 43–52.
- Güzelbey İH., Eraslan Y., Doğru MH. Numerical investigation of different airfoils at low reynolds number in terms of aerodynamic performance of sailplanes by using XFLR5. *Karadeniz Fen Bilimleri Dergisi* 2018; 8: 47–65.
- Hussein E., Azziz H., Rashid F. Aerodynamic study of slotted flap for NACA 24012 airfoil by dynamic mesh techniques and visualization flow. *Journal of Thermal Engineering* 2021; 7: 230–9.
- Jacobs EN. Airfoil section characteristics as affected by variations of the reynolds number. *NACA Report* 1937; 586.
- Maldonado V., Peralta N., Gorumlu S., Ayele W., Santos D. Aeroelastic response of a propulsive rotor blade with synthetic jets. *Journal of Fluids and Structures* 2021; 107: 103411.
- Menter FR. Two-equation eddy-viscosity turbulence models for engineering applications. *AIAA Journal* 1994; 32: 1598–1605.
- Metzinger CN., Chow R., Baker JP., Cooperman AM., van Dam CP. Experimental and computational investigation of blunt trailing-edge airfoils with splitter plates. *AIAA Journal* 2018; 56: 3229–39.
- Mohamed OS., Ibrahim AA., Etman AK., Abdelfatah AA., Elbaz AMR. Numerical investigation of Darrieus wind turbine with slotted airfoil blades. *Energy Conversion and Management: X* 2020; 5: 100026.
- Mohamed WMW., Ravindran NP., Rajendran P. A CFD Simulation on the performance of slotted propeller design for various airfoil configurations. *CFD Letters* 2021; 13: 43–57.

- Ohashi M., Morita Y., Hirokawa S., Fukagata K., Tokugawa N. Parametric study toward optimization of blowing and suction locations for improving lift-to-drag ratio on a Clark-Y airfoil. *Journal of Fluid Science and Technology* 2020; 15: JFST0008–JFST0008.
- Ozkan GM. Control of the flow in the near wake of an airfoil at full stall using fixed trailing-edge plates. *Experimental Thermal and Fluid Science* 2021; 122: 110296.
- Öztürk M., Demircan T. Yüksek sıcaklığa ulaşan elektronik elemanların etkin bir şekilde soğutulması. *Osmaniye Korkut Ata Üniversitesi Fen Bilimleri Enstitüsü Dergisi* 2022; 5: 612–631.
- Ramzi M. Numerical study of long separation bubble on slotted thick airfoil. *PAMM* 2018; 18: e201800411.
- Shabur A., Khan AH., Resan NS. Computational fluid dynamics analysis on turbulent kinetic energy distribution of NACA 0018 airfoil at two Reynolds number. *Research and Reviews: Journal of Mechanics and Machines* 2021; 4: 1–12.
- Singh MK., Dhanalakshmi K., Chakrabartty SK. Navier-stokes analysis of airfoils with gurney flap. *Journal of Aircraft* 2007; 44: 1487–1493.
- Song K. Numerical investigation of flatback airfoils drag and noise reduction by a splitter plate. *IOP Conf Ser: Earth Environ Sci* 2020; 495: 012081.
- Storms BL., Jang CS. Lift enhancement of an airfoil using a gurney flap and vortex generators. *Journal of Aircraft* 1994; 31: 542–547.
- Timmer WA. Two-dimensional low-reynolds number wind tunnel results for airfoil NACA 0018. *Wind Engineering* 2008; 32: 525–537.
- Wang JJ., Li YC., Choi K-S. Gurney flap-Lift enhancement, mechanisms and applications. *Progress in Aerospace Sciences* 2008; 44: 22–47.